EXHIBIT H

Rendering Human Skin

Clemens Brandorff

Abstract

Like Joel L. Swerdlow stated:" Computer Graphic artists will capture the holy grail of animation when they bring virtual skin to life."(Unmasking skin, National Geographic, Nov 2002, 112-134). Rendering human skin is a matter which poses many problems. Some of the problems are, that skin appearence varies not only across individuals, but varies spatially and temporary whithin a single individual too. Furthermore emotions, health, physical activity and cosmetics affect the visual appearence of skin for example. And skin appearence is highly affected by the position of the camera and the lighting enviroment used due to the subsurface scattering within the skin. In this paper I will give a short overview over the anatomy and optics of skin, and will present some techniques on rendering human skin, that have been developed in the past. This techniques include Analytical Reflectance Models, Numerical Reflectance Models, and Image-based approaches. Level of Detail for skin and asperity scattering will be discussed too.

CR Categories: I.3.7 [Computing Methodologies]: Computer GraphicsThree-Dimensional Graphics and Realism

Keywords: Human Skin, Rendering, Subsufrace Scattering, BSS-RDF, BRDF, Asperity Scattering, Level of Detail, Monte Carlo Method

1 Introduction

To gain a deeper understanding about human skin is the goal of many different research areas, for example medicine, cosmetics, coomputer graphics, etc. For the area of computer graphics it is desirable to render photorealistic images for movies, games, etc. To achieve auch results it is important to understand the anatomy and its impact on light transport within the skin. Chapter two and three try to give some understanding about the anatomy and the parts which influence the light transport within the skin. It is there that we will see that skin is a multy layered translucent material, where each layer has distinct optical and physical properties. In Chapter four I will describe some techniques that try to render and/or describe translucent materialn, multy layered translucent materials or skin directly. Because most of the works described try to render translucent materials (not only skin) most of the pictures show other materials than skin. The techniques are roughly divided into three categories: Analytical Redlection based models, Numerical Redlection based models and Image-based approaches.The techniques presented vary not only in rendering-time, but also in interactivity, biologically/physically correctness and the number and type of the parameters. In section 4.5 I will present the skin form a "level of detail view", which is important since there are characteristical features witch are needed to give rendered skin a photorealistical look. As a last technique, but especially important for the perception of human faces, I want to present Asperity Scattering nin section 4.6.
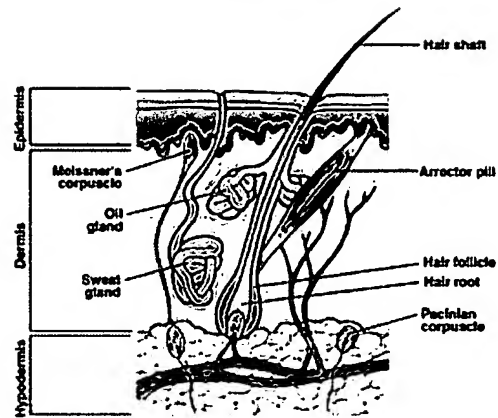
Skin: Cross Section

Figure 1: crossection of human skin

2 Anatomy of human skin

In this section I will present the anatomy and physiology relevant for rendering human skin. For the more interested reader, the anatomy and function of the human skin are well described in [Ernst G. Jung 2003]. To have a deeper unsderstanding on human skin I will give a short description on the parts and functions of the skin subdivided into three major parts: the epidermis, the dermis and the hypodermis(figure 1).

2.1 The Epidermis

The epidermis is the outermost part of the skin and is subdivided into five layers (from superficial to the deepest) the stratum corneum, the stratum luceum, the stratum granulosum, the stratum spinosum, the stratum germinativum. The main substance concerning absorption and scattering of light are the melanin pigments.

- **Stratum Corneum** This outermost layer, also called the horny layer, is mostly comprised of polygonal flattened dead cells filled with mature keratinocyte that are pushed towards the surface and gradually die and break apart. It is covered with a layer of sebum, a oily-waxy material produced by the sebaceous glands, that keeps the layer flexible and waterresistant.

- **Stratum Lucidum** Also called the clear layer it represents a transition from the underlaying stratum granulosum to the above stratum corneum.

- **Stratum Granulosum** Also called the granular layer. The granules accumulated in the keratinization process contain lipides whose role is to help prevent fluid loss from the body.

- **Stratum Spinosum** Also called the spiny layer, it consists of several layers of newly created cells from the stratum germinativum.

• **Stratum Germinativum** The stratum germinativum consists of a single layer of cells necessary in the regeneration process of the above layers. Mitotic processes in this layer create new cells that migrate upwards through the different layers in the progressive maturation process of keratinization.

Melanin Pigments are the most important part of the epidermis considering optics. Melanin pigments are found in skin, hair and eyes. These pigments are produced in the stratum germinativum and are also present in the stratum spinosum, the upper layers contain no melanin. These pigments protect the material of the underlying mitotic cells from ultra violett rays. Therefore the absorption spectrum increases towards shorter wavelenghts to act as a protective filter. There are two types of melanin: eumelanin and pheomelanin. The black to dark-brown eumelanin is found in skin, black hair and the retina of the eye. The yellow to reddish-brown pheomelanin is found in red hair. All individuals have varying content of eumelanin whereas the pheomelanin is only found in inviduals with the corresponding genetic trait.

2.2 The Dermis

The main function of the dermis is thermoregulation, physical strength, and providing the epidermis with nutrients. About 90 percent of the skin mass comes from the dermis. The dermis mostly consist of collagen fibres (approx. 70 percent), fatty tissue, nerves, lympatic vessels and blood vessels. The most important factor considering optics is the hemoglobin in its variations within the blood. The dermis is subdivided into two regions: the papillary dermis and the reticular dermis.

• **Papillary Dermis** The main function of this region is the thermoregulation. Depending on the bloodflow through this region (decreased/increased) this region either conserves or dissipates heat. An other important function is to supply nutrients to the epidermis. The ateries in this layer form two plexus, the deep plexus located at the transition to the hypodermis and the superficial plexus, located about 1-2mm below the epidermis.

• **Reticular Dermis** This region contains irregular shaped connectivity tissue, and most of the structures that give skin its strength and elasticity. Also glands, hair follicles, blood vessels and sensory nerve endings are contained in this region.

Hemoglobin, Carotene and Billirubin The number of blood vessels, and the colour of the blood mostly influence the appearence of the skin in this layer (particulary the Caucasians, since they got fewer eumelanin in their epidermis, that fact allows more light to reach the layer of the dermis). The most important factor considering optics in the blood is the hemoglobin. The hemoglobin itself is categorized in three groups: oxy-hemoglobin (HbO2) when its bound to oxygen, deoxy-hemoglobin (Hb) when its bound to nothing and carboxy-hemoglobin(HbCO) when its bound to carbon monoxide. The absorption spectrum is different of all three kinds of hemoglobin. Carotene, an orange pigment, contributes to the overall skin colour, but much less than hemoglobin, or melanin and therefore could be neglected. Its presence in the body mostly depends on food consumption. Billirubin is the waste product from the breakdown of worn out bloodcells. Red bloodcells contain hemoglobin which is broken down into heme and globin. Heme then is converted into billirubin which is transported through the blood vessels to the liver where it is disposed. Excessive levels of billirubin stain yellow the fatty tissue in the skin which happenes when the liver isnt working properly for example.

2.3 Hypodermis

The hypodermis allows the skin relative free movement over the underlying tissues. It consists of two layers, the superficial fascia and the deep fascia. It plays no role in the optics of the skin.

2.4 Other parts of the human skin

The parts described here, are superficial attributes of the skin that are important for the Level of detail and the aperity scattering.

• **Hair Follicles** Hair follicles consist of its internal and external root sheath. Each follicle has associated arrector pilli muscles to errect the hair(for thermoregulation). The base of the follicle originates in the papillary dermis containing capillaries to provide nutrients to the follicle.

• **Sweat Glands** Sweat Glands are simple coiled tubular glands which open at the skin surface (approx. 0.4mm diameter). They produce a watery secretion to cool down the skin surface.

• **Sebaceous Glands** Secaceous Glands produce an oily liquid secretion called sebum and are attached (mostly) to hair follicles. These glands are found all over the body (approx. 100/cm2) except the palms and the foot soles, but are most prominent on the face, scalp, chest and back (400-900/cm2). Excess of sebum secretion is a cause of acne. The exact function still remains unknown, although some have suggested it has antibiotical and antifungal properties along with helping prevent water loss.

3 Optics of Skin

In this section i will present formulas that describe the spectral absorption and scattering of the parts of the human skin, that play a role in rendering. As stated in the previous section, the most important part of the epidermis considering optics is the melanin, and for the dermis it is the hemoglobin within the blood in its variations.

The independend parameter λ denotes the wavelenght of the light.

3.1 Baseline Skin Spectral Absorption Coefficient

There are two measurements for the Baseline Skin Spectral Absorbtion Coefficient $\mu_{a.skinbaseline}$. The first one according to [S.L.Jaques 1998] is based on skin of a bloodless rat. The second was generated with in vitro neonatal skin samples by [Saidi].

$$\mu_{a.skinbase}(\lambda) = 0.244 + 85.3 * e^{(-\frac{\lambda - 154}{66.2})} \ [cm^{-1}] \qquad (1)$$

$$\mu_{a.skinbase}(\lambda) = (7.84 * 10^8) * (\lambda^{-3.255}) \ [cm^{-1}] \qquad (2)$$

3.2 Melanin Spectral Absorption Coefficient

The melanin spectral absorption coefficient, $\mu_{a.mela}$, is based on a single melanosome, and exhibits stronger absorption at shorter wavelenghts. [S.L.Jaques 1998] approximates the coefficient by:

$$\mu_{a.mela}(\lambda) = (6.6 * 10^{11}) * (\lambda^{-3.33}) \ [cm^{-1}] \qquad (3)$$

3.3 Epidermis Spectral Absorption Coefficient

The epidermis spectral absorption coefficient, $\mu_{a.epi}$, depends on the previously defined $\mu_{a.skinbaseline}$ and $\mu_{a.mela}$, taking into account how much melanin pigments are present in an individual. f_{mela} denotes the volume fraction of melanosomes in an individual skin.

$$\mu_{a.epi} = (f.mela) * (\mu_{a.mela}) + (1 - fmela) * (\mu_{a.skinbase}) \quad [cm^{-1}]$$
(4)

According to [S.L.Jaques 1998] f.melanosome varies approximatly:

- 0.01-0.06 for light-skinned adults
- 0.11-0.16 for moderately pigmented adults
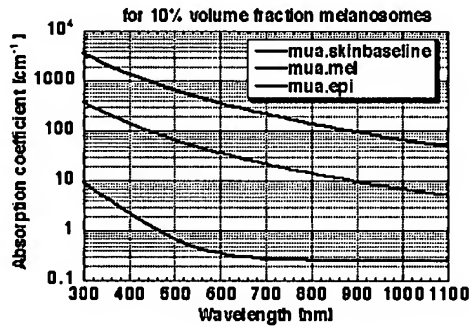- 0.18-0.43 for darkly pigmented adults

Figure 2: Absorption coefficient of epidermis, $f_{mela} = 0.1$

3.4 Epidermis Spectral Scattering Coefficient

The backward scattering of light in the visible spectrum of the epidermis is only 5 percent of the incident radiation, and therefore is very weak (A according to [R. Anderson and Parish 1981]). The mean cosine of the deflection angle g, due to a scattering event varies in the range of 0.7-0.95 for skin tissue. [M.J.C. van Gemert and Star 1989] report that the Henyey-Greenstein phase function (see Appendix) fits well the scattering behaviour of the epidermis. They report values g between 0.71 at 300nm and 0.78 at 540nm varying linearly with wavelength. The reduced scattering coefficient depends on the scattering coefficient of the dermis, $\mu_{s.epi}$, and the mean cosine phase function, g_{epi}.

$$\mu_{sp.epi} = (\mu_{s.epi}) * (1 - g_{epi}) \quad [cm^{-1}]$$
(5)

Due to the thinness of the epidermis and the keratin fibres which are similar to the collagen fibres of the dermis, $\mu_{sp.epi}$ could be approximated by the dermis spectral scattering coefficient.

3.5 Blood Spectral Absorption Coefficient

The blood spectral absorption coefficient $\mu_{a.blood}$ is mostly influenced by the variations of hemoglobin. The spectral absorption coefficient of oxy-hemoglobin exhibits two characteristic absorption bands, first at 420nm and in the range of 545-575nm it forms a

very characteristic W-pattern. The spectral absorption coefficient of deoxy-hemoglobin tend to exhibit lower absorbtion at higher wavelengths (see figure 3)
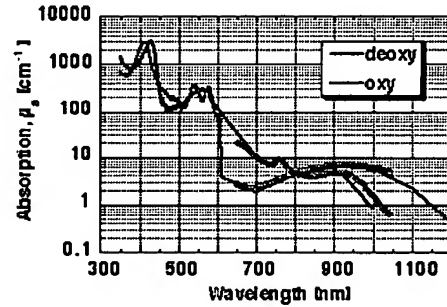
Figure 3: Absorption coefficient of whole blood RED = oxy-hemoglobin, BLUE = deoxy-hemoglobin.

3.6 Dermis Spectral Absorption Coefficient

The dermis spectral absorption coefficient, $\mu_{a.dermis}$ takes into account how much blood is present in the skin (the volume fraction f_{blood}) and the $\mu_{a.blood}$. The blood is not evenly distributed in the skin, but for an external observer it doesn't matter much. According to this description of $\mu_{a.dermis}$ is [S.L.Jaques 1998]:

$$\mu_{a.dermis} = f_{blood} * \mu_{a.blood} + (1 - f_{blood})\mu_{a.skinbase} \quad [cm^{-1}] \quad (6)$$

a typical value for f_{blood} is 0.02

3.7 Dermis Spectral Scattering Coefficient

[1981] states that the Dermis Spectral Scattering Coefficient $\mu_{s.dermis}$ increases with decreasing wavelenght, with red light penetrating deeper than blue light. Due to the collagen fibres, the scattering coefficient could be described by a combination of Rayleigh and Mie scattering (see Appendix). It is dominated by Rayleigh scattering for smal scale structures at short wavelenghts and by Mie scattering for the fibres at larger wavelenghts.

The Mie scattering in the dermis (and skin) can be mimicked by [1998]:

$$\mu_{sp.Mie}(\lambda) = (2x10^5)(\lambda^{-1.5}) \quad [cm^{-1}] \quad (7)$$

The Rayleigh scattering in the dermis (and skin) is [1998]

$$\mu_{sp.Rayleigh}(\lambda) = (2x10^{12})(\lambda^{-4}) \quad [cm^{-1}] \quad (8)$$

The reduced scattering $\mu_{sp.dermis}$ is a combination of the Raleigh and Mie scattering [1998].

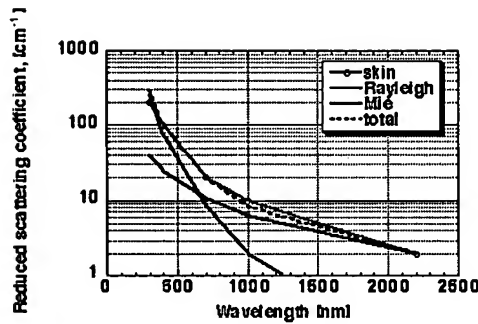$$\mu_{sp.dermis} = \mu_{sp.Rayleigh} + \mu_{sp.Mie} \quad [cm^{-1}] \quad (9)$$

Figure 4: $\mu_{sp.dermis}$, RED = tissue data, GREEN = Mie, BLUE = Rayleigh, BLACK DASHED LINE = Mie + Rayleigh

4 Rendering Techniques

Skin rendering techniques can be divided into two categories: Reflectance based models, and image based rendering techniques. Let us take a look into the reflectance models first. This category can be further divided into analytical and numerical models. After presenting Reflectance models in realtime and non realtime and image based approaches i will discuss some techniques, not only used in skin rendering, to archive better results rendering skin. These techniques will be Level Of Detail and Asperity Scattering.

4.1 Analytical Skin Reflection Models

At analytical models, assumptions are made to derive an analytical solution for the light transport in skin. Some models treat the skin as a homogeneous material (what, in an biological sense, it is not) and use a diffusion approximation. Others view the skin as a layered material and use Kubelka-Munk-like functions to describe the optical transport. The possibility of inverting an analytical model (that is: going from reflectance to skin parameters) is an andvantage, because there are applications where there is a need of such an inversion of the model (for example medical applications). A big advantage for the analytical models is that they are much more computational efficient than numerical models. Analytical models, often, can be transformed into numerical models by combining them with an adequate scattering model in order to produce Bidirectional Reflectance Distribution Functions (BRDFs) or Bidirectional Surface Scattering Reflectance Distribution Functions (BSSRDFs) if needed (see Apendix). The difference between BRDF and BSSRDF are illustrated in figure 5 and figure 6. Both figures use the same resources (model and bumb-maps), note the differences in the softer appearence of the BSSRDF, the BSSRDF results in colour bleeding, and softer shadown under the nose.

Stam [2001] presents a reflection model for a skin layer, bounded by two rough surfaces. He derived an analytical approximation to multiple scattering using an ordinate approximation of the radiative equation. The model uses only one layer, but accounts for multiple anisotropic scattering whithin this layer, and makes use of the BRDF framework. This technique is much faster than a Monte Carlo approach, and does not suffer from the noisy artifacts produced by a Monte Carlo technique. This reflection model was implemented by the authors as a MAYA plugin, and they stated that the implementation is noticable better than the Lambert shader. Figure 7 shows a comparison of this shader(right) and a picture generated with the technique proposed by Hanrahan and Krueger
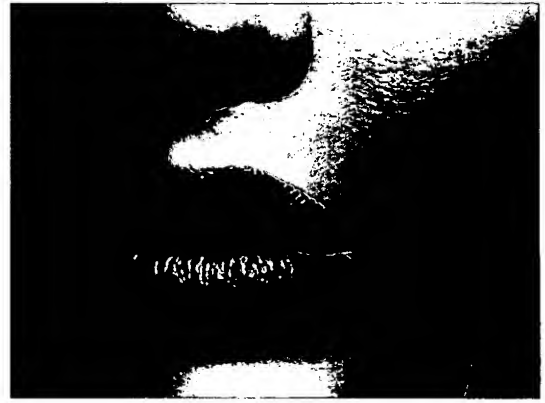

Figure 5: BRDF

Figure 6: BSSRDF

[1993](left), note that the Hanrahan and Krueger model had to be brightened up to be able to compare it to the two others due to facht that the Hanrahan and Krueger model only uses single scattering.

Cotton and Claridge [1996] [2002] and Claridge and Precec [2003] use a predictive model based on the Kubelka-Munk theory (see Appendix). This model predicts that the colours of the skin lie on a simple curved surface patch within the three-dimensional colour space, bounded by two physiologically meaningful axes, one corresponding to the amount of melanin within the epidermis, the other corresponding to the amount of blood within the dermis. This model assumes that scattering in the epidermis is negligible, and that Beer's Law (see Appendix) can be applied to describe the attenuation in the epidermis. The dermis has a high scattering coefficient, and therefore cannot be modeled with Beer's Law. The model of light transport they use is generalized for n layers, but they effectively use two layers: the reticular dermis and the papillary dermis (divided into upper and lower). Mie-scattering is used to model the reticular dermis, while Rayleigh-scattering is used to model the reticular dermis. This model is designed to help clinicans in performing early diagnosis of maligant melanoma (for example with a device like the SIAscope in figure 8), and does not concern itself with rendering the results.

The next model in this category is a model proposed by Jensen et al [2002] [2001], that uses the complete BSSRDF along with a diffusion approximation to model subsurface scattering instead of
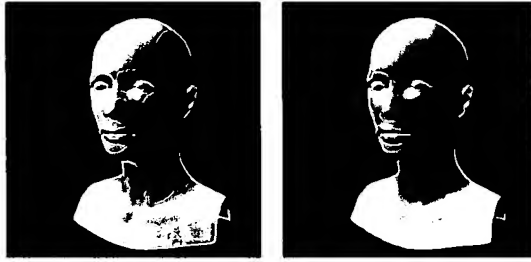
Figure 7: A comparison of the shader developed by Stam (right), and a picture generated with the technique proposed by Hanrahan and Krueger(left).

Figure 8: SIAscope a certified commercial device developed using the model of skin colouration described in the papers of Cotton and Claridge

Figure 9: Dipole diffusion approximation

using BRDF. The BSSRDF allows to simulate effects which BRDF cannot, for example colour bleeding within materials and diffusion of light across shadow boundaries and silhouettes(compare figure 5 and figure 6). This model combines the exact solution for a single scattering with a dipole point source diffusion approximation to account for multiple scattering, The authors mention that light distribution in highly scattering media tends to become isotropic since each scattering event blurs the light, even if the initial light source and the phase function used are highly anisotropic. The diffusion equation has a simple solution in case of a single isotropic point of light source in an infinite medium [2001]. A more accurate approximation is the dipole diffusion approximation, where the volumetric light source is modelled by using two point sources. One (the positive real) is located beneath the surface at a distance z_r, the other (the negative virtual), is located above the surface at a distance of z_v (see figure 9). This technique yields good results compared to a full Monte Carlo simulation (compare figure 10 and figure 11). The BSSRF simulation took 4 minutes to render while the full Monte Carlo simulation took 1250 minutes.

The BSSRDF is very costly to evaluate since the incident flux has to be sampled on the surface. With volumetric or aera light sources this sampling has to be performed both at the light and the translucent object surface. In [2001] **Jensen and Buhler** present a technique to speed up the computation for shading translucent objects.
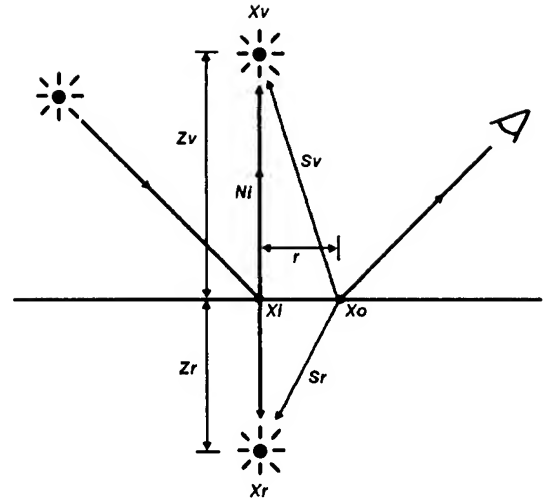
This speed gain is archived by decoupling the computation of irradiance at the surface from the evaluation of the scattering within the material by a two-pass algorithm. In the first pass the irradiance is computed at selected points on the surface. In the second pass the dipole diffusion equatation is solved using the precomputed irradiance values. The irradiance values from the first pass are stored in an octree datastructure, which has to be recomputed every time the illumination changes with respect to the translucent object.

Donner and Jensen [2005] propose a extension to the dipole diffusion approximation approach. Dipole diffusion approximation assume that the material is homogeneous, and semi-infinite thick. Altough the dipole method proposed by [Jensen et al. 2001] has ben modified by [Jensen and Buhler 2002] and [Mertens et al. 2003], the underlying theory remained unchanged. The improvement proposed in this paper is called multipole diffusion approximations (figure 12 schematically compares the dipole method to the multipole method), which accounts for light scattering within thin slabs.

This method is generalized for multiple layers with different optical parameters for each layer and arbitrary layer thickness. It is based on a novel frequency space application of the Kubelka and Munk Theory. This technique is both accurate and efficient and easily intergrated into existing implementations based on the dipole diffusion approximations. Figure 13 compares the rendering of a prachment (approx. 1mm thick) illuminated from behind, rendered with the dipole method, multipole method and the expensive Monte Carlo method. The diople method predicts a transmittance of 3.3%, while the multipole method predicts 22.6% which is quite the sam as the Monte carlo method which predicts 21.5%.

Donner and Jensen [2006] proposed another technique (in shetch form) for rendering human skin: a spectral analytical model. Their model accounts for both surface and subsurface scattering, and uses only four parameters, the amount of oil, melanin and hemoglobin in the skin (see figure 14 for a schematical overview of the parts used in this model). They generate spectral diffusion profiles by modelling the skin as a two layer translucent material using the mutipole diffusion approximation they proposed earlier [Donner and Jensen 2005].

Figure 10: A marble bust rendered with BSSRDF

Figure 11: A marble bust rendered with full Monte Carlo simulation

The epidermis absorbs light according to the amount and type of melanin (eumelanin, pheomelanin) in this layer. The light absorbed in the dermis is defined by the amount and type of the hemoglobine (oxyhemoglobine and deoxyhemoglobine) in this second layer. To account for the surface scattering from an oily layer (the sebum layer) they used the Torrence -Sparrow BRDF [Torrance and Sparrow 1967]. This model is physically quite correct and yields very good results as seen in figure 15. With only four, easy to understand, parameters it is quite easy to handle for artists which are not familiar with the underlying technical and mathematical features of this technique.

4.2 Numerical Skin Reflection Models

Numerical models try to model the full light transport in skin tissue. They are capable of accuratly describing the anatomy of skin and therefore produce a very good approximation of its reflectance. The quality depends directly on the anatomy model choosen. Numerical models can be used in BRDF or BSSRDF frameworks, altough BSSRDF including full multiple scattering simulation might be computationally very expensive. Therefore Monte Carlo methods are often used to solve the light transport. But there are considerable drawbacks using the Monte Carlo method, for example the method is hightly computationally complex and the sampling nature of the Monte Carlo method results in noise which is not satisfactory for the smooth appearence of skin.Furthermore Numerical Skin Reflection Models let the intuitive connection between the parameters and the physiology vanish and are not easily invertible.

Hanrahan and Krueger [1993] present a model where a Monte Carlo method is used to perform the full multiple scattering simulation. In this model the subsurface scattering in a layered material is handled in terms of a one-dimensional linear transport theory. Four layers are modelled here, namely the epidermis, the dermis, the pigment and the blood. The optical properties for each layer are the index of refraction, the absorption cross section, the scattering cross section, the layer depth, the scattering phase function and the mean cosine of the phase function. The used parameters are independent with respect to the wavelength, which is biologically not correct. Furthermore they assume that the boundaries of the
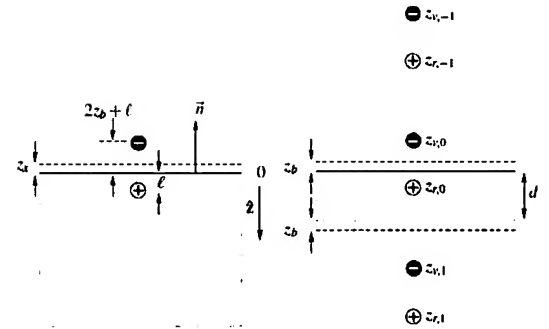

Figure 12: Dipole configuration for semi-infinite geometry (left), and the multipole configuration for thin slabs (right).

different layers are flat, which is biologically not correct as well, especially the outermost, the horny layer. They also consider only one level of interreflection instead of multiple interreflections before the light leaves the layer. BRDF is used here instead of the more accurate BSSRDF because BSSRDF is just too expensive in a Monte Carlo framework.

Ng and Li [2001] present a model similar to Hanrahan and Krueger [1993] using a Monte Carlo framework as well, but including another layer, the sebum layer. Sebum is found almost over the whole body, causing the skin to look more specular. The improvement can be seen in figure 16. Optical properties are loosly connected to Jaques [1998] and therefore more biologically accurate.

As a last model of this category and the most biologically correct presented here, i want to present a model proposed by **Meglinsky and Matcher** [2002] [2003]. They use stochastic Monte Carlo simulation to model optical radiation propergation in skin. The computational model used here is similar to the one used by Hanrahan and Krueger [1993], but they use seven layers with their various thickness namely: stratum corneum, living epidermis, papillary dermis, upper blood net dermis, reticular dermis, deep blood net dermis, and subcutaneous fat. They take into ac-

Dipole model   Multipole model
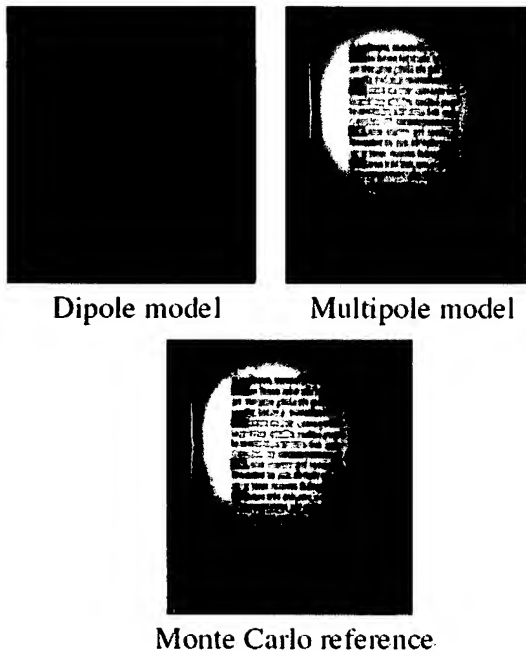
Monte Carlo reference

Figure 13: A piece of parchment illuminated from behind. Note, how the dipole model (left) underestimates the amount of transmitted light, while the multipole model (middle) almost matches the reference image computed using Monte Carlo photon tracing (right).

Figure 14: Two layer skin model

Caucasian   Asian   African

Figure 15: Results of the model proposed by Donner and Jensen [2006], upper row renderings, lower row photographs

count that each layer has variations in thickness and try to model that variations as quasi-random periodic surfaces (see figure 17) [2001a] [2001b] [2002]. The optical parameters they use have been collected from numerous literature sources. This model, altough the most comprehensive and biological accurate, has not been implemented in computer graphics, because of its very high computational costs when using BSSRDF, which should be used to produce important effects in smaller scale as mentioned before.

4.3 Real-Time Skin Reflection Models

The volume or subsurface light is a computationally very expensive task to simulate, and therefore it is not well suited for interactive or realtime rendering. After the paper from Jensen et al. [2002], several works tried to accomplish this task in realtime. Most of that works use the dipole diffusion approximation.

Kniss et al. [2002] described a qualitative interactive volume shading model that captures volumetric light attenuation effects to produce volumetric shadows and the qualitative appearence of subsurface scattering. This model does not need specifications of the optical properties of the material, because it relys on empirical data of observations of the appearence of volumetric materials. It is capable of producing typical subsurface effects like bleeding colours and diffusion of light accros shadow boundaries. Multiple scattering produces indirect lighting whose qualitative effects diffusion of light through the volume. This diffusion is modelled by using a Gaussian blur, that averages the incoming light within a cone with an apex angle θ in the direction of the light. The user-specified parameter is the transport colour, which is the colour the indirect light
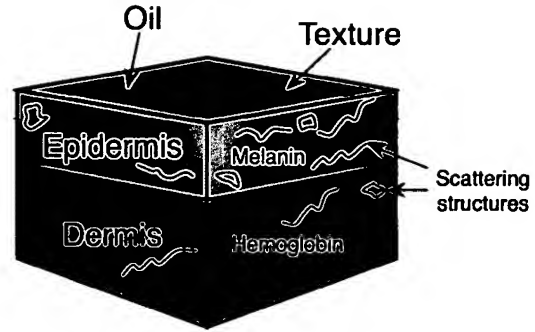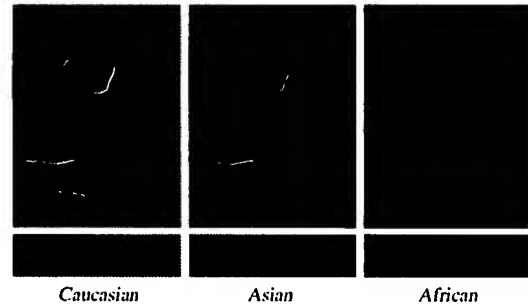
will become as it is attenuated by the material. This model needs three buffers, two for the attenuation of the light, and one for the accumulation of the light for the observer. Two passes are required to perform the bluring and the number of samples depends on the number of texture-units available.

Lensch et al. [2002] describe an interactive method to render translucent objects with arbitraty viewport or illumination. Their approach to model the blurring of incident illumination is to factor the light impulse response on the surface into a low frequency global component and a high frequency local component. The smooth global component models the subsurface scattering at large distances and the high frequency component accounts for the detailed local part. This technique works as follows:

1. Incident illumination is computed and projected into a texture atlas.

2. The smooth global part is computed by projecting the illumination to the mesh vertices and multiplying the vertex irradiance vector with a vertex-to-vertex throughput factor matrix [2002].

3. The detailed local part is computed by filtering the incident illumination map with spatially varying 7x7 texel-to-texel filter kernels.

4. The global and local parts are merged together.

The merging of the local and global parts cannot be accomplished by simply blending them together. The influence of the low frequency part has to be reduced at small scattering distances and therefore smooth blending has to be ensured where the influence of the local part ends. The authors state that the preprocessing time
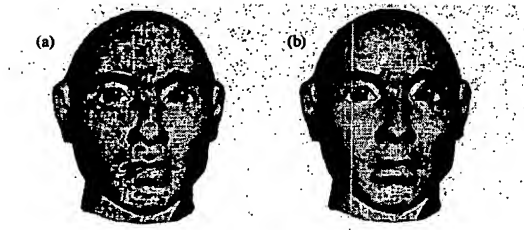
Figure 16: Without sebum (a), with sebum (b)

Figure 17: An example fo a pseudo-random surface

of the models they used was between three and ten minutes. The horse model, with uniform marble and with added veins, in figure 18 has 10000 vertices and could be rendered at an interactive framerate of 2.3 frames per second(on a dual 1.7 GHz Xeon PC with 1GB of RAM, using a GeForce3).
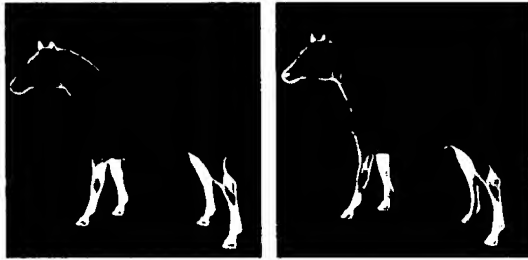

Figure 18: The horse model with uniform marble (left) and with added veins (right). The structures in the head and leg areas are clearly noticable.

Hao et al. [2003] describe a model to approximate BSSRDF within a local illumination context, exploiting the locality of the diffusion approximation. It is an empirical model that aims at mimicking multiple subsurface scattering. The local illumination process is divided into two stages: The traditional local lighting stage and a scatter-bleeding stage. A neighbourhood of a vertex x_o is computed in a preprocessing stage. The neighbours are defined to include all vertices x_i that lie within the effective scattering range. This range varies according to the relative refraction index η the absorption coefficient σ_o and the scattering coefficient σ_s. This neighbourhood eliminates all vertices whose impact is too small on the irradiance due to subsurface scattering at x_o. The outgoing radiance at a point is computed by an integral over all incoming light directions and surface aera, and is expressed as a summation over all vertices in the neighbourhood of x_o. At run time the outgoing radiance is interpolated via a Quarternion-based vector interpolation. This algorithm has a complexity of $O(n)$, where n is the number of vertices in a polygonal mesh. However the precomputation is quite expensive, and has to be redone when the mesh or the material parameters are changed. The authors state that the preprocessing stage takes about

40 min. for a 150K mesh with 200 light directions (that results in 200 precomputed integrals). The model in figure 19 has 14521 vertices, and was rendered at 181 frames per second without subsurface scattering, and at 79.1 frames per second with subsurface scattering. The difference between the three horses rendered with subsurface scattering is the neigbourhood of x_o (from a to c 10%, 20%, 30% vertices):

Figure 19: (a)(upper left) without subsurface scattering 181 frames per second,(b)(upper right),(c)(lower left),(d)(lower right) with subsurface scattering 79.1 frames per second

Carr et al. [2003] describe a model similar to the one in [Lensch et al. 2002] with modifications to allow a full GPU implementation of subsurface scattering. Dynamic modifications of light or reflectance parameters are possible. Geometry is fixed and precomputation of all throughput factors between interacting surfaces has to be done before on the CPU. They solve the matrix radiosity system completly on the GPU using a Jacobi technique given precomputed form factors using support for floating point texture formats. The model uses a multi-resolution mesh atlas applied to a surface cluster hierarchy, taking advantage of the hardware mipmapping capability. The algorithm needs to perform three passes on the GPU. The model in figure 20 (right side with subsurface scattering) has 7232 faces, and has been rendered with 40 frames per second on a GeForce FX 5900.

All models so far prohibit interactive modifications of the geometry. The model proposed by **Mertens et al.** [2003] allows interactive modifications of lighting, viewport, subsurface scattering properties and object geometry. Since BSSRDF is dependent on the object geometry, the authors state that it is reasonable to remove the solid

Figure 20: Without subsurface scattering (left), with subsurface scattering(right)

Figure 21: The Max Plank model, back-lit

angle dependencies from the BSSRDF term since multiple scattering diffuses the illumination. The model for the BSSRDF without solit angle dependencies $R_d(x_i, x_o)$ should be adabtable to different materials and should be efficient. They also use the dipole diffusion approximation over the full simulation.

Dachsbacher and Stamminger [2003] introduced an extension to standart shadow maps called Translucent Shadow Maps (TSM). Standard shadow maps are rendered from the light's point of view and store the depth of the closest surface to the light source at each texel. TSMs store in addition to that the irradiance and surface normal at each texel. To speed up the rendering the evaluation of the subsurface scattering is divided into two componens like [Lensch et al. 2002], a local component and a global component. This is done because to compute the local component one can use more costly techniques. The local component is computed by weighting and summing up the texels in the neighbourhood of the exitant point x_o. The global component is computed using a dipole diffusion approximation between x_o and x_i (the incident point) and is stored in the TSM. The irradiance gathering at x_o is computed using a hi-erarchical filter based on a mipmap of the TSM. This algorithm is able to render complex objects at interactive frame-rates, and simpler objects in real-time. For example the Max Plank model in the figure 21 with 25044 vertices, 49999 triangles, was rendered at a frame-rate of 14.2 frames per second on their hardware (P4 2.4Ghz, ATI 9700);

The technique used in the movie "Matrix Reloaded" (see Image-Based Skin Rendering) was implemented on graphics hardware in real-time by ATI researchers **Pedro Sander et al.** [2004]. Their algorithm works as follows:

1. Render the diffuse illumination to a 2-d light map.

2. Compute and store shadows in the light map.

3. Blur the light map.

4. Finally render the mesh using the blurred 2-d light map to provide diffuse illumination:

The authors note that these steps are straightforward to implement using fragment shaders and renderable textures. For the shadows, a shadow map algorithm was used and the according texels in the diffuse light map are dimmed. To achieve soft shadows and the effects subsurface scattering creates the diffuse light map was blurred using a poisson disc blur. They discarded the raytracing of the translucent
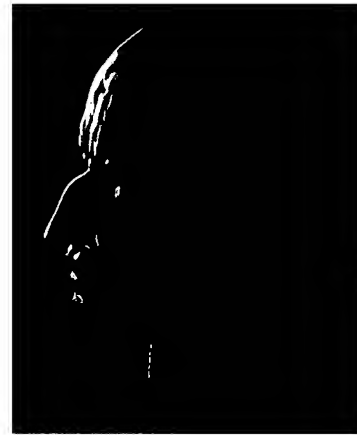
parts as ears in the original paper. Instead of the raytracing the authors state that they archieved similar effects using a varying kernel size of the poisson disc blur (increasing the kernel size at regions that are translucent).Figure 22 shows the result of this technique, and the corresponding diffuse light map.

Figure 22: Result of the Technique proposed by Sander et al. [2004](left), and corresponding diffuse light map (right)

4.4 Image Based Skin Rendering

To generate effects like self shadowing, inter-reflections and multiple scattering is very difficult with the models described so far. Image-based techniques attempt to tackle this problem from a different angle. They aquire data needed to render skin from images. The image-based approaches suffer, like all image-based approaches from high memory consumption, incident illumination captured in the images and the difficulty of modifying the results.

Georghiades et al. [1999] and **Debevec et al.** [2000] aquire the reflectance field from a series of images. Devebec generates images from two fixed cameras while varying the illumination direction using a device they called "light stage". They are able to generate images from the original viewpoints, under any illumination condition, by computing linear combinations of the original images. It is also possible to perform a re-lighting with sampled natural lighting enviroments, called "light probes", due to the additive nature of light. But they must still use a skin reflectance model along with a geometric model in order to render the subject under novel viewports.

Malzbender et al. [2001] describe a technique to gather the bidirectional texture function (BTF) of a surface by collecting multiple images of a static camera under varying lighting conditions. This technique is called polynomial texture map (PTM). To approximate the surface colour under varying lighting conditions the coefficients of a biquadratic polynomial is stored per texel. This technique works in real-time using graphics hardware.

Now i want to present a commercial technique, used in the famous movie "Matrix Reloaded", proposed by **Borshukov and Lewis** [2003]. They needed to create completly photorealistic renderings of their actors. For the facial surface details they used a 100-micron resolution scan of a plaster cast mold of the actors faces. These scans resulted in models with extremly high polygon count (approx. 10 million triangles, see figure 23 part 1). A low res 5K-quad model was created from the highresolution models by a software called Paraform. To render the skin they choose an image-based approach. Like the former mentioned techniques they used static cameras with varying illumination to derive an approximate analytical BRDF(see figure 23 part 2 for the setting and part 3 for the result). They realized that they could not ignore the subsurface scattering for skin if they want to achieve highly photorealistic results. They developed a fairly inexpensive and easy to implement technique for that. The result of the diffuse illuminatopn reflecting off the face in the camera direction is stored in a 2-d light map(see figure 23 part 4). Light diffusion is then approximatly simulated in the image domain. For objects like ears, where light is able to pass directly through, they employed a traditional ray-tracing approach to archieve the desired translucency. These components were combined and a raytracer was able to produce highly photorealistic results (compare part 6 and 7 in figure 23).

4.5 Level Of Detail

Level of Detail was first proposed in computer graphics by Clark [1976]. Level of scale are usually divided into three structures namely: macro-structure, meso-structure and micro-structure. The different structures are usually represented by different rendering algorithms. For skin that is:

- Macro-structure : BRDF,BSSRDF
- Meso-structure : bumpmapping
- Micro-structure : displacement mapping.

The rendering algorithm is choosen as a function of distance, viewing angle, and the bump frequency in the bumpmap. Now I want to present the three structures for skin, and their responding rendering techniques.

Macro-structure

This level is a geometric model represented as a polynomial mesh, curved surface, etc. It can be acquired by a 3D scanning device, photographs, a geometric modelling application or any other acquisition technique. Geometric-based representations usually consider direct illumination and self shadowing.

Meso-structure

The meso-structure consists of geometric details, finer, but still visible. They are represented as a bumpmap or by a technique that computes self shadowing of the bump map called horizon mapping proposed by Max [1988].

Micro-structure

Figure 23: Pictures of the technique used in the movie "Matrix Reloaded". 1: high resolution model. 2: camera setting to aquire the image-based BRDF. 3: result of the setting from picture 2. 4: 2-d light map. 5,6: synthetic images of 2 actors. 7: real image corresponding to the synthetic image in 6.

The micro-structure-level cosists of micro facetes that are not individually visible, but contribute to the overall BRDF. BRDF considers direct illumination but it takes into account self shadowing and masking effects of the micro structure. It also accounts for indirect illumination resulting from light that scatteres between the micro facetes and subsurface scattering in the material.

Aquiring the skin meso-structure

The skin meso-structure mostly consists of ridges, furrows, hair follicle openings and sweat gland openings. This lattice-type pattern changes from individuum to individuum and within a single individuum in different regions (see figure 24) and due to aging (skin elasticity decreases over time). This pattern influences the overall BRDF of the skin, it even is directly visible under various lighting conditions. Therefore skin meso-structure is crucial to render realistic looking skin. There are different techniques to aquire the skin geometric structure like molds, laser scanners, photographs etc.

Haro et al. [2001] describes a technique where they use latex molds, used in cosmetology, to aquire the exact structure of different parts of the skin. This samples are quite small (about the size of an euro-cent coin). Therefore a texture synthesis algorithm needs to be applied to generate high resolution maps for the structure. It is important to avoid visual discontinuities between the different
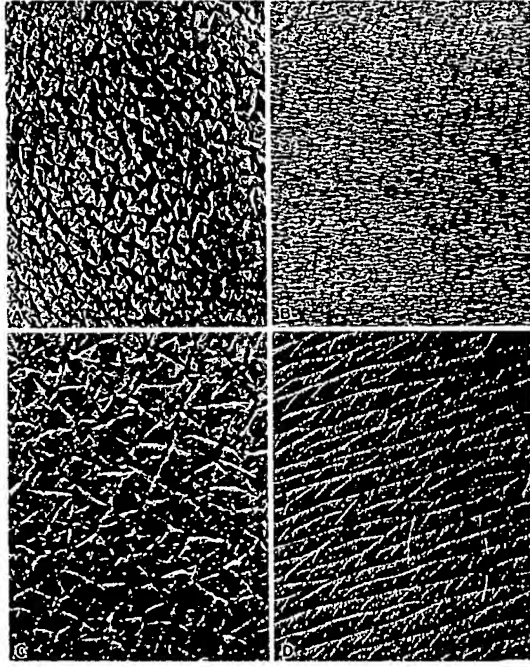
Figure 24: Surface structure from (A) the elbow, (B) antecubital fossa, (C) knee, and (D) popliteal fossa of the same subject

zones of the skin. The authors use random-multi-resolution splines to hide the seams across different patches. Curved boundaries suppress the highly noticable visual artifacts that seams between rectangular boundaries create. A per-pixel bump mapping is used in conjunction with a Lafortune shading model [Kubelka 1948] that approximates the BRDF of the skin to render the model in real-time.

A simple model is proposed by **Ishii et al.** [1990] [1993]. They use a Vonroi diagram to represent the different skin cells and use the optical scattering properties of the skin layer to perform rendering. Geometric diversity is archieved using a pseudo-fractal subdivision in the Vonroi procedure. Vonroi-based textures are able to produce patterns similar to skin cells [T. Ishii and Toriwaki 1993] (see figure 25 and compare to figure 24).
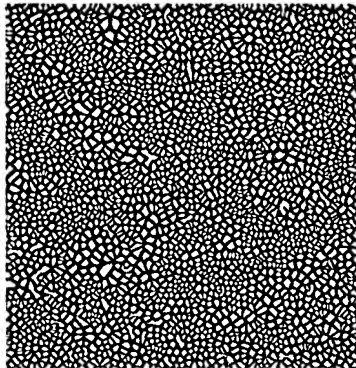

Figure 25: Example of a vonroi bump map

4.6 Asperity Scattering

Asperity scattering occours when the material is covered with a thin layer of sparse scatterers like dust or hair. Skin, especially facial skin of children and women is covered with small light hair (see figure 26). **Koenderink and Pont** [2003] describe a simple model for Asperity Scattering. They assume a layer of constant thickness Δ with a uniform distribution of scatterers. The propability of a ray entering from a direction l, and scattering back towards the viewer in direction e is derived in [Koenderink and Pont 2003]:

$$f(l,e) \approx \frac{p(-le)\frac{\Delta}{\lambda}}{(nl)(ne)} \qquad (10)$$

where: $\Delta \ll \lambda$,

$p(-le)$: phase function,

Δ: layer thickness,

λ: mean free path.

In the case of isotropic scatterers:

$$f(l,e) \approx \frac{\frac{\Delta}{4\pi\lambda}}{(nl)(ne)} \qquad (11)$$

Asperity Scattering mostly affects the contours and the body shadows, and therefore it might have a strong influence on the perception of faces.

5 Conclusion

This section is divided into a conclusion for non-real-time techniques, for real-time techniques, and Image-based approaches. Level of detail is commonly used nowadays, but is nevertheless very important to render photorealistic skin while reducing computation cost. The skin features described in the Level of detail section are crucial to render photorealistic skin. More research has to be done to develop tools for artists to easy generate these features procedurally. Asperity scattering is a very important feature for displaying human faces, and should not be neglected when trying to render human faces.

Non-Real-Time

In the sector of Non-Real-Time skin rendering, the results of the techniques developed so far, are quite good and have acceptable rendering times on the harware they used. The rendering times should be drastically reduced using modern hardware which goes for highly parallel processing. The sector where more research and developement have to be done, is the developement of intuitive tools for the artists to use this techniques, because the parameters for this techniques often require alot of knowledge of the technical features of underlying techniques used. As far as i can say, the technique proposed by [Donner and Jensen 2006] could be the most promising, because the results look very good, and the parameters are few and easy to understand. Since this technique was only proposed in form of a sketch, the authors did not mention rendering times.

Real-Time

In the sector of real-time skin rendering many techniques have been proposed. They differ in performance, interactivity and quality. For some one who wants to render skin in real-time it is a hard task to

Figure 26: Example of Asperity Scattering. The hair cover is sparse, and the hair is very thin and short, it is hardly noticeable in most circumstances except grazing illumination like here.

choose the technique which fits their needs best. Like with non-real-time techniques the real-time techniques lack proper tools for artists who arent familiar with the technical and mathematical aspects of the technique used.

With the launch of Windows Vista, in early 2007, which includes DirectX 10, and the corresponding graphics cards like Nvidias GeForrce 8xxx series it should be possible to use more complex real-time rendering algorithms, since memory access is improved, and a new shader is incorporated (geometry shader), that should be able to help generating a skin-meso structure in real geometry without increasing the CPU load. But I think that it will still take some time until computer graphic programmers and scientists are able to make use of the new features and develop new techniques which the develpoers of DirectX never thought of yet.

Image-Based Approaches

The image based approached described in this work have aswell nice results, but they have a big drawback: The generation of the BRDF/BSSRDF form a set of images require some hardware which could be a financial problem for developers. But if we look at the results generated in the movie "Matrix Reloded" I have to say these are great looking.

6 Appendix

6.1 Phase Functions

A phase function, also called scattering function, describes the scattered distribution of light after a ray hits a particle in a layer. The layer is composed of a medium with particles in a suspension within it. Usually it is assumed that the particles are uniformly distributed within that medium, and that the medium and the particles are both independantly homogeneous. In general, phase functions are four dimensional functions of the incoming and outgoing directions $p(\omega_i, \omega_o)$. If the particles are randomly orientated, the phase function can be reduced to a function of the phase angle between the two directions $p(cos(\alpha)) = p(\omega_i, \omega_o)$. The choice of a particular phase function depends on the ratio of the wavelength and the particle size involved.

Rayleigh Phase Function

Rayleigh phase function is used when the particle size is a bit smaller than the wavelength of light. It is can model the scattering behaviour of cigarette smoke and dust for example. For the skin it is used to model the scattering behaviour of the small scale collagen fibres in the dermis.

The Rayleigh pase function is:

$$P_{Rayleigh}(cos\alpha) = \frac{3}{4}(1 + (cos\alpha)^2) \qquad (12)$$

Mie Phase Function

Mie phase function is used when the particles are about the size of the wavelenght of light. It can model the behaviour of waterdrops in fog. For the skin it is used to model the scattering of longer wavelengths in the dermis. There are two different Mie phase fuctions which I want to present here. The murky Mie, used when the particle density is high , and the hazy Mie , used when the particle density is sparse.

The murky Mie is:

$$P_{murkyMie} = 1 + 50(\frac{1 + cos\alpha}{2})^3 2 \qquad (13)$$

The hazy Mie is:

$$P_{hazyMie} = 1 + 9(\frac{1 + cos\alpha}{2})^8 \qquad (14)$$

Henyey-Greenstein Phase Function Another Mie scattering approximation is the Henyey-Greenstein phase function. It takes an asymmetry parameter g, the mean cosine of the phase function, which goes from strong retro-reflection $g = -1$ to strong forward scattering $g = 1$. Isotripic scattering is achived with $g = 0$.

The Henyey-Greenstein Phase Function is:

$$P_{Henyey-Greenstein}(cos\alpha, g) = \frac{1 - g^2}{(1 + g^2 - 2gcos\alpha)^{\frac{3}{2}}} \qquad (15)$$

6.2 Bidirectional Surface Scattering Reflectance Distribution Function (BSSRDF)

For materials that inhibit subsurface scattering, that is light enters the material, is scattered within the material and then leaves the surface at a different location. The BSSRDF S relates to the differential reflected radiance dL_o at an exitant location x_o in direction ω_o to the differential incident flux $d\phi_i$ at an incident location x_i from direction ω_i. Note that the reflectance functions presented here are dependant on the wavelength λ. That parameter is omitted for convenience and is always assumed implicitly.

$$S(x_i, \omega_i; x_o, \omega_o) = \frac{dL_o(x_o, \omega_o)}{d\phi_i(x_i, \omega_i)} \qquad (16)$$

The amount of radiance leaving a point x_o can be expressed as

$$L_o(x_o, \omega_o) = \int_A \int_\Omega S(x_i, \omega_i; x_o, \omega_o) L_i(x_i, \omega_i)(n_i \omega_i) d\omega_i dA(x_i) \qquad (17)$$

The BSSRDF is an eight-dimensional function and is very computationally expensive to evaluate.Many authors have noted that single scattering accounts for a small percentage of the total outgoing radiance in highly scattering materials. That leads to a simplyfied BSSRDF $R_d(x_i, x_o)$ called diffuse BSSRDF which is only four-dimensional.

6.3 Bidirectional Reflectance Distribution Function (BRDF)

When light hits a surface, its is partly absorbed. The rest is scattered back into the enviroment by the properties of the material. The BRDF is defined as the differential reflected radiance in the outgoing directionper differential indicent irradiance in the incoming direction. The BRDF is an six-dimensional approximation of the more accurate BSSRDF (see graphics below):

$$f_r(\theta_i, \phi_i; \theta_o, \phi_o) = \frac{dL_o(\theta_o, \phi_o)}{dE_i(\theta_i, \phi_i)} \qquad (18)$$

for physical accuracy the BRDF must ensure the Helmholtz law of reciprocity:

$$f_r(\omega_i \rightarrow \omega_o) = f_r(\omega_o \rightarrow \omega_i) \qquad (19)$$

6.4 Beer's Law

Beers's Law, also called Beer-Lambert law, or Beer-Lambert-Bouguer law describes an empirical relationship that relates the absorption of light to the properties of the material through which the light is travelling.

There are several ways to describe this law (i will only present two of them here).
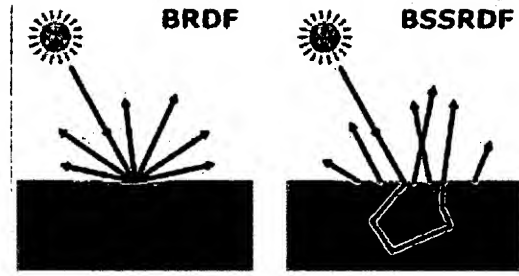
$$A = \alpha l c \qquad (20)$$

Figure 27: BRDF vs. BSSRDF (from http://en.wikipedia.org)

$$\frac{I_0}{I_1} = 10^{-\alpha l c} \qquad (21)$$

A is absorbance

I_0 is the intensity of the incident light

I_1 is the intensity after passing through the material

l is the distance that the light travels through the material (the path length)

c is the concentration of absorbing species in the material

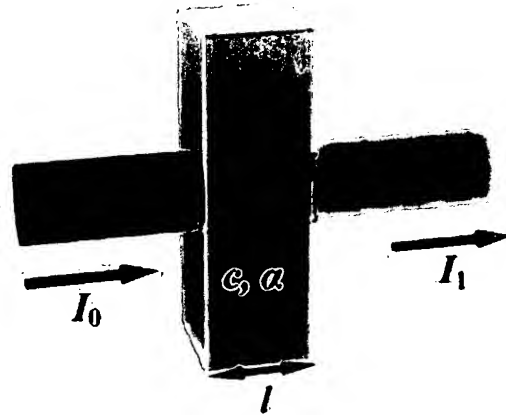α is the absorption coefficient or the molar absorptivity of the absorber

Figure 28: Diagram of Beer absorption of a beam of light as it travels through a cuvette of size l.(from http://en.wikipedia.org)

6.5 The Kubelka-Munk Model

This model is an early attempt to model layered material, consisting of layers of different coloured paint. To obtain an analytical solution some assumptions have been made:

Particles are small in comparison to the material thickness.

The composition of each layer is homogeneous (uniform colour and scattering properties).

The top layer is irradiated by incident light uniformly from all directions and light exiting each layer after scattering is also uniformly distributed.

The assumptions limit this model for physically-based rendering, but some authors still used it to model skin or pigmented materials in computer graphics.

For a single layer the reflection coefficient R and the transmission coefficient T of the layer are given by the Kubelka-Munk equatations. Note that these equatations are wavelenght-dependant.

$$R(\beta,K,d,\lambda) = \frac{(1-\beta^2)(e^{Kd}-e^{-Kd})}{(1+\beta)^2 e^{Kd} - (1-\beta)^2 e^{-Kd'}} \quad (22)$$

$$T(\beta,K,d,\lambda) = \frac{4\beta}{(1+\beta)^2 e^{Kd} - (1-\beta)^2 e^{-Kd'}} \quad (23)$$

d: depth of the layer.

$\sigma_a(\lambda)$: attenuation or absorbtion cross section of the layer at a particular wavelength.

$\sigma_s(\lambda)$: scattering cross section of the layer at a particular wavelenght.

$s = 2\sigma_s(\lambda)$

$K = \sqrt{k(k+2s)}$

$\beta = \sqrt{\frac{k}{k+2s}}$

$k = 2\sigma_a(\lambda)$

References

A. GEORGHIADES, P., AND KRIEGMAN, D. 1999. Illumination-based image synthesis: creating novelimages of human facesunder differing pose and lighting. In *Procdeedings Workshop on Multi-View Modeling and Analysis of Visual Scenes*, 47–54.

BORSHUKOV, G., AND LEWIS, J. P. 2003. Realistic human face rendering for "the matrix reloaded". In *SIGGRAPH '03: ACM SIGGRAPH 2003 Sketches & Applications*, ACM Press, New York, NY, USA, 1–1.

CARR, N. A., HALL, J. D., AND HART, J. C. 2003. Gpu algorithms for radiosity and subsurface scattering. In *HWWS '03: Proceedings of the ACM SIGGRAPH/EUROGRAPHICS conference on Graphics hardware*, Eurographics Association, Aire-la-Ville, Switzerland, Switzerland, 51–59.

CLARIDGE, E., AND PRECEC, S. 2003. An inverse method for the recovery of tissue parameters from colour images. In *Information Processing in Medical Imaging*. 306–317.

CLARK, J. H. 1976. Hierarchical geometric models for visible surface algorithms. *Commun. ACM 19*, 10, 547–554.

DACHSBACHER, C., AND STAMMINGER, M. 2003. Translucent shadow maps. In *EGRW '03: Proceedings of the 14th Eurographics workshop on Rendering*, Eurographics Association, Aire-la-Ville, Switzerland, Switzerland, 197–201.

DEBEVEC, P., HAWKINS, T., TCHOU, C., DUIKER, H.-P., SAROKIN, W., AND SAGAR, M. 2000. Acquiring the reflectance field of a human face. In *SIGGRAPH '00: Proceedings*

of the 27th annual conference on Computer graphics and interactive techniques, ACM Press/Addison-Wesley Publishing Co., New York, NY, USA, 145–156.

DONNER, C., AND JENSEN, H. W. 2005. Light diffusion in multilayered translucent materials. In *SIGGRAPH '05: ACM SIGGRAPH 2005 Papers*, ACM Press, New York, NY, USA, 1032–1039.

DONNER, C., AND JENSEN, H. W. 2006. A spectral shading model for human skin. In *SIGGRAPH '06: ACM SIGGRAPH 2006 Sketches*, ACM Press, New York, NY, USA, 147.

E. CLARIDGE, S. COTTON, P., AND MONCRIEFF, M. 2002. From colour to tissue histology: physics based interpretation of images of pigmented skin lesions. In *Medical Image Computing and Computer-Assisted Intervention*. September, 730–738.

ERNST G. JUNG, I. M. 2003. *Dermatologie*. Thieme Verlagsgruppe.

HANRAHAN, P., AND KRUEGER, W. 1993. Reflection from layered surfaces due to subsurface scattering. In *SIGGRAPH '93: Proceedings of the 20th annual conference on Computer graphics and interactive techniques*, ACM Press, New York, NY, USA, 165–174.

HAO, X., BABY, T., AND VARSHNEY, A. 2003. Interactive subsurface scattering for translucent meshes. In *SI3D '03: Proceedings of the 2003 symposium on Interactive 3D graphics*, ACM Press, New York, NY, USA, 75–82.

HARO, A., ESSA, I. A., AND GUENTER, B. K. 2001. Real-time photo-realistic physically based rendering of fine scale human skin structure. In *Proceedings of the 12th Eurographics Workshop on Rendering Techniques*, Springer-Verlag, London, UK, 53–62.

JENSEN, H. W., AND BUHLER, J. 2002. A rapid hierarchical rendering technique for translucent materials. In *SIGGRAPH '02: Proceedings of the 29th annual conference on Computer graphics and interactive techniques*, ACM Press, New York, NY, USA, 576–581.

JENSEN, H. W., MARSCHNER, S. R., LEVOY, M., AND HANRAHAN, P. 2001. A practical model for subsurface light transport. In *SIGGRAPH '01: Proceedings of the 28th annual conference on Computer graphics and interactive techniques*, ACM Press, New York, NY, USA, 511–518.

KNISS, J., PREMOZE, S., HANSEN, C., AND EBERT, D. 2002. Interactive translucent volume rendering and procedural modeling. In *VIS '02: Proceedings of the conference on Visualization '02*, IEEE Computer Society, Washington, DC, USA, 109–116.

KOENDERINK, J., AND PONT, S. 2003. The secret of velvety skin. *Mach. Vision Appl. 14*, 4, 260–268.

KUBELKA, P. 1948. New contributions to the optics of intensity light-scattering materials, part i. In *Journal of the Optical Society of America*. May, 448–457.

LENSCH, H. P. A., GOESELE, M., BEKAERT, P., KAUTZ, J., MAGNOR, M. A., LANG, J., AND SEIDEL, H.-P. 2002. Interactive rendering of translucent objects. In *PG '02: Proceedings of the 10th Pacific Conference on Computer Graphics and Applications*, IEEE Computer Society, Washington, DC, USA, 214.

MALZBENDER, T., GELB, D., AND WOLTERS, H. 2001. Polynomial texture maps. In *SIGGRAPH '01: Proceedings of the*

28th annual conference on Computer graphics and interactive techniques, ACM Press, New York, NY, USA, 519–528.

MAX, N. 1988. Horizon mapping: shadows for bump-mapped surfaces. In *The visual Computer*. July, 109–117.

MEGLINSKI, I., AND MATCHER, S. 2001. The analysis of spatial distribution of the detector depth sensitivity in multi-layered inhomogeneous highly scattering and absorbing medium by the monte carlo techniques. In *Opt. Spectrosc.*, 654–659.

MEGLINSKI, I., AND MATCHER, S. 2001. Modelling the sampling volume for the skin blood oxygenation measurements. In *Med. Biol. Eng. Comput.*, 44–50.

MEGLINSKI, I., AND MATCHER, S. 2002. Quantitative assesment of skin layers absorption and skin reflectance spectra simulation in the visible and the near-infrared spectral regions. In *Physiol. Meas.*, 741–753.

MEGLINSKI, I., AND MATCHER, S. 2003. Computer simulatiion of the skin reflectance spectra. In *Comput. Methods Programs Biomed.*, 179–186.

MERTENS, T., KAUTZ, J., BEKAERT, P., SEIDELZ, H.-P., AND REETH, F. V. 2003. Interactive rendering of translucent deformable objects. In *EGRW '03: Proceedings of the 14th Eurographics workshop on Rendering*, Eurographics Association, Aire-la-Ville, Switzerland, Switzerland, 130–140.

M.J.C. VAN GEMERT, S.L. JAQUES, H. S., AND STAR, W. 1989. Skin optics. In *IEEE Transactions on Biomedical Engineering*.

NG, C. S.-L., AND LI, L. 2001. A multi-layered reflection model of natural human skin. In *CGI '01: Computer Graphics International 2001*, IEEE Computer Society, Washington, DC, USA, 249–256.

PEDRO SANDER, D. G., AND MITCHELL, J. L., 2004. Real-time skin rendering on graphics hardware.

R. ANDERSON, B. P., AND PARISH, C. 1981. The optics of human skin. In *The Journal of Investigative Dermatology*.

S. COTTON, E. C. 1996. Developing a predictive model of human skin colouring. In *Proceedings of SPIE Medical Imaging*, 814–825.

SAIDI, I. *Transcutaneous Optical Measurement of Hyperbilirubinemia in Neonates*. PhD thesis, Rice University.

S.L.JAQUES, 1998. Skin optics. Oregon Medical Laser Center News. http://omlc.ogi.edu/news/jan98/skinoptics.htm.

STAM, J. 2001. An illumination model for a skin layer bounded by rough surfaces. In *Proceedings of the 12th Eurographics Workshop on Rendering Techniques*, Springer-Verlag, London, UK, 39–52.

T. ISHII, T. KURACHI, T. Y. S. Y., AND TORIWAKI, J. 1990. Rendering the surface of skin using vonroi-division. In *ISPJ SIGNotes Computer Graphics and Cad*.

T. ISHII, T. Y., AND TORIWAKI, J. 1993. A generation model for human skin texture. In *Proc. CG Internationam '93: Communicating with Virtual Worlds*, 139–150.

TORRANCE, K., AND SPARROW, E., 1967. Theory for off-specular reflection from roughened surfaces. J. Opt. Soc. Am.